

# Full $\mathcal{O}(\alpha)$ Radiative Corrections to High-Energy Compton Scattering<sup>†</sup>

S. DITTMAIER

*Fakultät für Physik, Universität Bielefeld, Germany*

## Abstract

Using computer-algebraic methods we derive compact analytical expressions for the virtual electroweak radiative corrections to polarized Compton scattering. Moreover the helicity amplitudes for double Compton scattering, which prove to be extremely simple in terms of Weyl-van der Waerden spinor products, are presented for massless electrons. The inclusion of a finite electron mass is described, too. Finally numerical results both for the purely photonic and the full  $\mathcal{O}(\alpha)$  electroweak corrections, which turn out to be of the order of 5 – 10%, are discussed for energies ranging from 10 GeV to 2 TeV.

November 1993

---

<sup>†</sup>Work partially supported by the Bundesminister für Forschung und Technologie, Bonn, Germany.

# 1 Introduction

Since the experimental discovery of the reaction  $e^-\gamma \rightarrow e^-\gamma$  by Compton [1] in 1923 this so-called Compton scattering has been of continuous theoretical interest. Among the numerous work on this subject we just mention the most basic representatives, e.g. the lowest-order cross-section calculated by Klein and Nishina [2], the virtual and real soft-photonic QED radiative corrections (RCs) by Brown and Feynman [3] as well as the hard-photonic corrections – also called double Compton scattering – by Mandl and Skyrme [4]. Recently these results have been completed by the virtual electroweak RCs [5] within the Glashow-Salam-Weinberg model as part of a more general treatment of gauge-boson production in electron-photon collisions [6].

The relatively clean environment of electron-photon collisions will provide an opportunity for further precision tests of the electroweak standard model, which are complementary to the ones obtained from electron-positron scattering, in the future. As proposed in [7] high-energetic photon beams can be produced via Compton backscattering of laser light off high-energy electrons. Moreover elastic electron-photon backscattering is well-suited as luminosity monitor for such an electron-photon collider in analogy to Bhabha forward scattering in electron-positron colliders. Consequently the Compton process represents one of the most important processes in this context.

In [5] the analytical results for  $e^-\gamma \rightarrow e^-\gamma$  are related to the generic ones obtained for  $e^-\gamma \rightarrow W^-\nu_e$ ,  $e^-\gamma \rightarrow Z$  [8] rendering the analytical expressions quite untransparent. On the other hand the kinematical simplicity of Compton scattering for energies at the electroweak scale ( $M_W \gg m_e$ ) promises a comparably simple structure for the electroweak RCs although intermediate steps of the calculations are lengthy. Therefore we have applied the computer-algebra packages *FeynArts* [9] and *FeynCalc* [10] for generating the one-loop amplitudes for  $e^-\gamma \rightarrow e^-\gamma$  and reducing them to scalar integrals, respectively. The scalar one-loop integrals have been evaluated by standard methods [11]. The rather transparent and short results obtained this way form the first part of this work.

In a second step we deal with double Compton scattering. Following closely the procedure of [12], where the hard-photonic bremsstrahlung to  $e^-\gamma \rightarrow W^-\nu_e$ ,  $e^-\gamma \rightarrow Z$  is discussed, we use the Weyl-van der Waerden spinor formalism for the construction of very compact helicity amplitudes in the case of non-collinear photon emission. The finite-mass effects of the electron are included afterwards.

Finally we present numerical results for the pure (virtual and real) photonic as well as for the full  $\mathcal{O}(\alpha)$  RCs to the integrated Compton cross-section both for polarized and unpolarized particles for energies ranging from 10 GeV to 2 TeV.

The paper is organized as follows: In Sect. 2 we set some conventions and give the polarized Born cross-sections. The virtual electroweak RCs and the real soft-photonic corrections are presented in Sect. 3. Section 4 completes these analytical results by the hard-photonic bremsstrahlung. We conclude with a discussion of the numerical evaluations in Sect. 5. Finally the appendix provides completing analytical expressions.

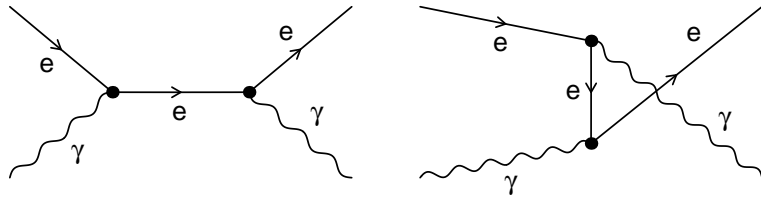


Figure 1: Tree diagrams for  $e^- \gamma \rightarrow e^- \gamma$ .

## 2 Notation and lowest-order cross-section

Since we use the notation and conventions of [5, 8] throughout it suffices to repeat here just the most basic definitions. The helicities of the incoming (outgoing) electron and photon are denoted by  $\sigma_e$  ( $\sigma'_e$ ) and  $\lambda_\gamma$  ( $\lambda'_\gamma$ ), respectively. The Mandelstam variables are given in the centre-of-mass system (CMS) by

$$s = 4E^2, \quad t = -4E^2 \sin^2 \frac{\theta}{2}, \quad u = -4E^2 \cos^2 \frac{\theta}{2} \quad (1)$$

where  $E$  represents the beam energy and  $\theta$  the scattering angle of the electrons (and also the photons). Here we already make use of the fact that we are interested in energies  $E \gg m_e$ . Consequently we neglect the electron mass whenever possible so that our results are valid for  $s, -t, -u \gg m_e^2$ . In this limit the two lowest-order Feynman diagrams<sup>1</sup> shown in Fig. 1 yield the following differential cross-sections

$$\left( \frac{d\sigma}{d\Omega} \right)_{\text{Born}} = \begin{cases} \alpha^2 \frac{1}{(-u)} & \text{for } \sigma_e = \sigma'_e = \pm \frac{1}{2}, (\lambda_\gamma, \lambda'_\gamma) = (\pm 1, \pm 1), \\ \alpha^2 \frac{(-u)}{s^2} & \text{for } \sigma_e = \sigma'_e = \pm \frac{1}{2}, (\lambda_\gamma, \lambda'_\gamma) = (\mp 1, \mp 1), \\ 0 & \text{otherwise.} \end{cases} \quad (2)$$

Hence both the electron and photon helicities are conserved in lowest order. Moreover there are two different symmetries: the Born cross-sections are invariant under simultaneous reversal of all helicities and the transition amplitudes<sup>2</sup> under the interchange ( $s \leftrightarrow u, \lambda_\gamma \leftrightarrow -\lambda'_\gamma$ ). The former is due to parity conservation, the latter expresses crossing symmetry.

## 3 Virtual electroweak and soft-photonic radiative corrections

Analogously to [5, 8] we calculate the virtual RCs in the 't Hooft-Feynman gauge applying the complete on-shell renormalization scheme as described in [13, 14], where a complete

<sup>1</sup>All Feynman diagrams of this work have been drawn with the help of *FeynArts* [9].

<sup>2</sup>The squared amplitudes and the cross-sections just differ by a trivial (flux) factor  $\propto 1/s$  which is not affected by this substitution.

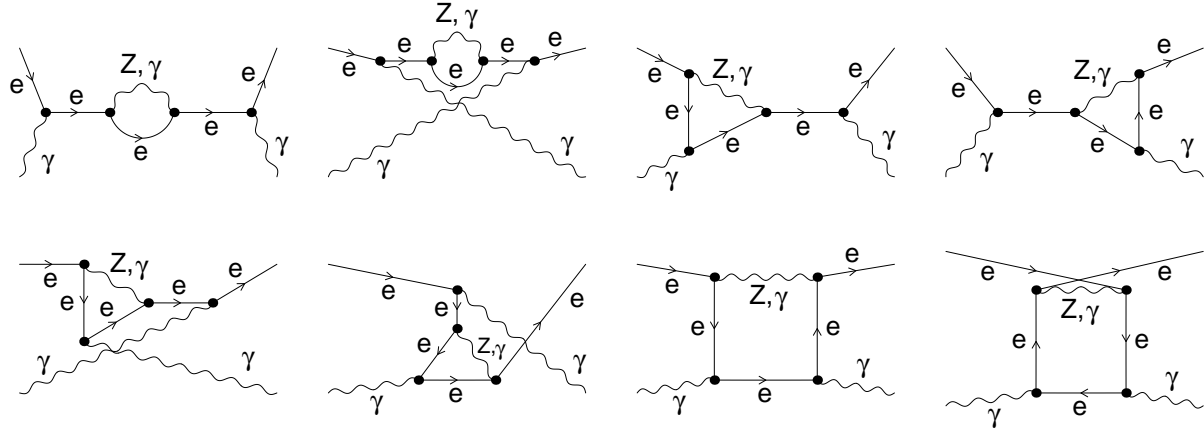


Figure 2: Feynman diagrams for the exchange of virtual photons and Z bosons.

list of the renormalization constants can be found. In particular the fields are normalized in such a way that the residues of all renormalized propagators are equal to one, i.e. self-energy contributions of external particles drop out. Expanding the squared transition-matrix element  $|\mathcal{M}|^2$  for  $e^- \gamma \rightarrow e^- \gamma$  up to  $\mathcal{O}(\alpha)$  and taking into account the soft-photonic bremsstrahlung factor  $\delta_{\text{SB}}$  yields for the differential cross-section

$$\begin{aligned} \left( \frac{d\sigma}{d\Omega} \right) &= \sum_{\sigma_e, \sigma'_e, \lambda_\gamma, \lambda'_\gamma} \frac{1}{4} (1 + 2\sigma_e P_e) (1 + \lambda_\gamma P_\gamma) \frac{1}{64\pi^2 s} \left[ |\mathcal{M}_{\text{Born}}|^2 (1 + \delta_{\text{SB}}) + 2\text{Re}\{\mathcal{M}_{\text{Born}}^* \delta \mathcal{M}\} \right] \\ &= \left( \frac{d\sigma}{d\Omega} \right)_{\text{Born}} (1 + \delta_{\text{virt}} + \delta_{\text{SB}}), \end{aligned} \quad (3)$$

where  $P_{e,\gamma}$  denote the degrees of beam polarization. Following the treatment of [5, 8] we decompose the virtual electroweak RCs, which are summed up in  $\delta_{\text{virt}}$ , into gauge-invariant subsets

$$\delta_{\text{virt}} = \delta_{\text{QED}}^{\text{virt}} + \delta_{\text{NC}} + \delta_{\text{W}}. \quad (4)$$

$\delta_{\text{QED}}^{\text{virt}}$  and  $\delta_{\text{NC}}$  include all contributions which are due to photon and Z-boson exchange, respectively. The corresponding Feynman diagrams are shown in Fig. 2. The remaining diagrams, which are shown in Fig. 3, contain virtual W bosons and form  $\delta_{\text{W}}$ .

The one-loop RCs vanish for all polarizations corresponding to a Born cross-section which is identically zero and vice versa so that we have to deal with the polarization combinations  $\kappa = \sigma_e = \sigma'_e$  and  $\rho = \lambda_\gamma = \lambda'_\gamma$  for  $\delta_{\text{virt}}$  only.<sup>3</sup> Moreover it turns out that each contribution to the virtual RCs respects crossing symmetry. Consequently we just have to give  $\delta_{\text{virt}}^\kappa(\rho = -1)$  and obtain the case  $\rho = +1$  via

$$\delta_{\text{virt}}^\kappa(\rho) = \delta_{\text{virt}}^\kappa(-\rho) \Big|_{s \leftrightarrow u}. \quad (5)$$

The following results for  $\delta_{\text{QED}}^{\text{virt},\kappa}(\rho)$ ,  $\delta_{\text{NC}}^\kappa(\rho)$ , and  $\delta_{\text{W}}^\kappa(\rho)$  have been obtained by the application of the computer-algebraic packages *FeynArts* [9] and *FeynCalc* [10]. The former program

<sup>3</sup>Note that instead of the proper values  $\kappa = \pm \frac{1}{2}$  we use the abbreviation  $\kappa = \pm$  in subscripts and superscripts to distinguish right- and left-handed quantities.

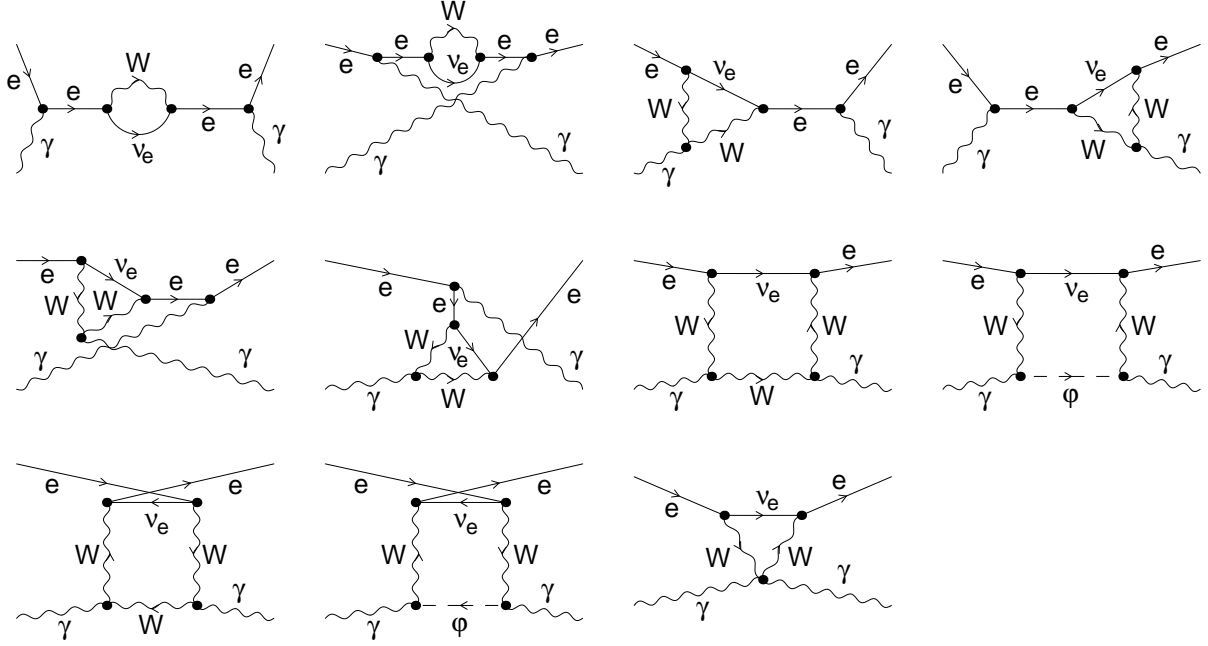


Figure 3: Feynman diagrams for the exchange of virtual W bosons.

generates the Feynman diagrams together with the corresponding transition-matrix elements for a given scattering process directly from the Feynman rules, the latter evaluates the Dirac algebra and reduces one-loop tensor integrals to scalar integrals. Finally these integrals, which are summarized in App. A, have been calculated by hand using the results and methods of [11].

### 3.1 Photon exchange

In order to regularize possible IR divergences we introduce an infinitesimal mass  $\lambda$  for internal photons if necessary. Inspecting the results for the virtual one-loop QED RCs

$$\begin{aligned} \delta_{\text{QED}}^{\text{virt},-}(-) &= \frac{\alpha}{\pi} \left\{ \log \left( \frac{s+i\varepsilon}{-\lambda^2} \right) \left[ 1 + \log \left( \frac{m_e^2}{-t} \right) \right] - \frac{1}{2} \log \left( \frac{-m_e^2}{u+i\varepsilon} \right) + \frac{1}{2} \log^2 \left( \frac{-m_e^2}{s+i\varepsilon} \right) \right. \\ &\quad \left. + \log \left( \frac{t}{s+i\varepsilon} \right) + \frac{t}{s} \log \left( \frac{t}{u+i\varepsilon} \right) + \frac{t^2}{2s^2} \log^2 \left( \frac{t}{u+i\varepsilon} \right) - \frac{3}{2} + \frac{4s^2+3t^2}{s^2} \zeta(2) \right\}, \\ \delta_{\text{QED}}^{\text{virt},+}(\rho) &= \delta_{\text{QED}}^{\text{virt},-}(-\rho), \end{aligned} \quad (6)$$

we find that it is entirely formed by logarithms.

### 3.2 Z-boson exchange

In [5, 8] it has been pointed out that the set of all Feynman diagrams which contain internal Z bosons form a gauge-invariant subset. The result for these contributions, which have been called *neutral current corrections*, reads

$$\begin{aligned} \delta_{\text{NC}}^-(-) &= \frac{\alpha}{\pi} \left( g_{\text{eeZ}}^- \right)^2 \left\{ \left( 1 - \frac{M_Z^2}{u} \right) \left( \frac{3}{2} + \frac{u}{s} + \frac{M_Z^2}{2u} - \frac{M_Z^2}{s} \right) \log \left( 1 - \frac{u + i\varepsilon}{M_Z^2} \right) - \frac{u}{s} \log \left( \frac{-t}{M_Z^2} \right) \right. \\ &\quad + \frac{(t + M_Z^2)^2}{s^2} \left[ \zeta(2) - \log \left( \frac{-t}{M_Z^2} \right) \log \left( 1 - \frac{u + i\varepsilon}{M_Z^2} \right) - \text{Li}_2 \left( \frac{u + i\varepsilon}{M_Z^2} \right) - \text{Li}_2 \left( 1 + \frac{t}{M_Z^2} \right) \right] \\ &\quad \left. - \frac{(s - M_Z^2)^2}{s^2} \left[ \log \left( \frac{-t}{M_Z^2} \right) \log \left( 1 - \frac{s + i\varepsilon}{M_Z^2} \right) + \text{Li}_2 \left( \frac{s + i\varepsilon}{M_Z^2} \right) \right] + \frac{M_Z^2}{s} - \frac{M_Z^2}{2u} - \frac{5}{4} \right\}, \\ \delta_{\text{NC}}^+(\rho) &= \delta_{\text{NC}}^-(-\rho) (g_{\text{eeZ}}^+ / g_{\text{eeZ}}^-)^2, \end{aligned} \quad (7)$$

where the electron-Z couplings are abbreviated by

$$g_{\text{eeZ}}^+ = \frac{s_W}{c_W}, \quad g_{\text{eeZ}}^- = \frac{s_W}{c_W} - \frac{1}{2s_W c_W}. \quad (8)$$

Note that the individual scalar integrals (see App. A) contain mass-singular logarithms of the electron which drop out in  $\delta_{\text{NC}}$ .

### 3.3 W-boson exchange

In contrast to the virtual QED and neutral current RCs the analytical results for the contributions caused by W-boson exchange do not simplify after inserting the explicit expressions for the scalar integrals. Therefore we introduce some abbreviations for these integrals which are explicitly given in App. A

$$\begin{aligned} \delta_W^-(-) &= \frac{\alpha}{4\pi s_W^2} \\ &\times \left\{ \frac{1}{2} + \frac{2u}{s} (1 - B_{tWW}) + \frac{u(2u - 3s) + M_W^2(2u - s)}{su} B_{u0W} + \frac{(u - s)(u + 2M_W^2)}{s^2} u t D_{ut} \right. \\ &\quad + \frac{u(s - u - 2M_W^2)}{s^2} \left[ t(C_{tWW} + C_{tWWW}) + 2u C_{uWW} - t M_W^2 D_{ut} \right] - \frac{(s - M_W^2)^2}{s^2} \\ &\quad \left. \times \left[ 2(s C_{sWW} + u C_{uWW} + t C_{tWWW}) + (s^2 - su - t M_W^2) D_{st} + (u^2 - us - t M_W^2) D_{ut} \right] \right\}, \\ \delta_W^+(\rho) &= 0. \end{aligned} \quad (9)$$

Recall that the comparably short results presented in (6), (7), and (9) have to be compared with lengthy and untransparent formulae of [8].

### 3.4 Soft bremsstrahlung

The soft-photonic bremsstrahlung factor  $\delta_{\text{SB}}$ , which is universal for all polarizations, can be simply cited from [8]

$$\delta_{\text{SB}} = -\frac{\alpha}{\pi} \left\{ \log \left( \frac{4\Delta E^2}{\lambda^2} \right) \left[ 1 + \log \left( \frac{m_e^2}{-t} \right) \right] + 2\zeta(2) + \text{Li}_2 \left( \frac{-u}{t} \right) + \log \left( \frac{m_e^2}{s} \right) + \frac{1}{2} \log^2 \left( \frac{m_e^2}{s} \right) \right\}. \quad (10)$$

Here  $\Delta E \ll E$  represents the soft-photon cut-off. In [5, 8] the QED corrections have been defined by

$$\delta_{\text{QED}} = \delta_{\text{QED}}^{\text{virt}} + \delta_{\text{SB}}. \quad (11)$$

Inspecting  $\delta_{\text{QED}}^{\text{virt}}$  and  $\delta_{\text{SB}}$  one easily verifies that both the IR-divergent terms ( $\log \lambda$ ) as well as the *Sudakov logarithms* ( $\log^2 m_e$ ) cancel in  $\delta_{\text{QED}}$ , and that the remaining mass-singular logarithms ( $\log m_e$ ) agree with the ones predicted by structure function methods [15].

## 4 Hard-photonic bremsstrahlung – double Compton scattering

In this section we deal with double Compton scattering, i.e. with the reaction

$$e^-(p_e, \sigma_e) + \gamma(k_\gamma, \lambda_\gamma) \rightarrow e^-(p'_e, \sigma'_e) + \gamma(k_1, \lambda_1) + \gamma(k_2, \lambda_2).$$

Using throughout the conventions and calculational techniques of [12], where the radiative processes  $e^-\gamma \rightarrow W^-\nu_e\gamma$ ,  $e^-Z\gamma$  have been discussed, we are able to present the results in a very compact manner.

### 4.1 Non-collinear photon emission

We first restrict our treatment to non-collinearly emitted photons so that we can neglect the electron mass for beam energies  $E \gg m_e$ . Owing to  $m_e = 0$  the electron helicity is conserved and we can define  $\kappa = \sigma_e = \sigma'_e$ . The originally  $2^4 = 16$  independent amplitudes  $\mathcal{M}^\kappa(\lambda_\gamma, \lambda_1, \lambda_2)$  are reduced to four independent polarization combinations by the following discrete symmetries:

$$\text{Bose symmetry: } \mathcal{M}^\kappa(\lambda_\gamma, \lambda_1, \lambda_2) = \mathcal{M}^\kappa(\lambda_\gamma, \lambda_2, \lambda_1) \quad \text{with } 1 \leftrightarrow 2, \quad (12)$$

$$\begin{aligned} \text{crossing symmetry: } \mathcal{M}^\kappa(\lambda_\gamma, \lambda_1, \lambda_2) &= \mathcal{M}^\kappa(-\lambda_1, -\lambda_\gamma, \lambda_2) && \text{with } \gamma \leftrightarrow 1, \\ &= \mathcal{M}^\kappa(-\lambda_2, \lambda_1, -\lambda_\gamma) && \text{with } \gamma \leftrightarrow 2, \end{aligned} \quad (13)$$

$$\text{parity conservation: } \mathcal{M}^\kappa(\lambda_\gamma, \lambda_1, \lambda_2) = -\mathcal{M}^{-\kappa}(-\lambda_\gamma, -\lambda_1, -\lambda_2)^*. \quad (14)$$

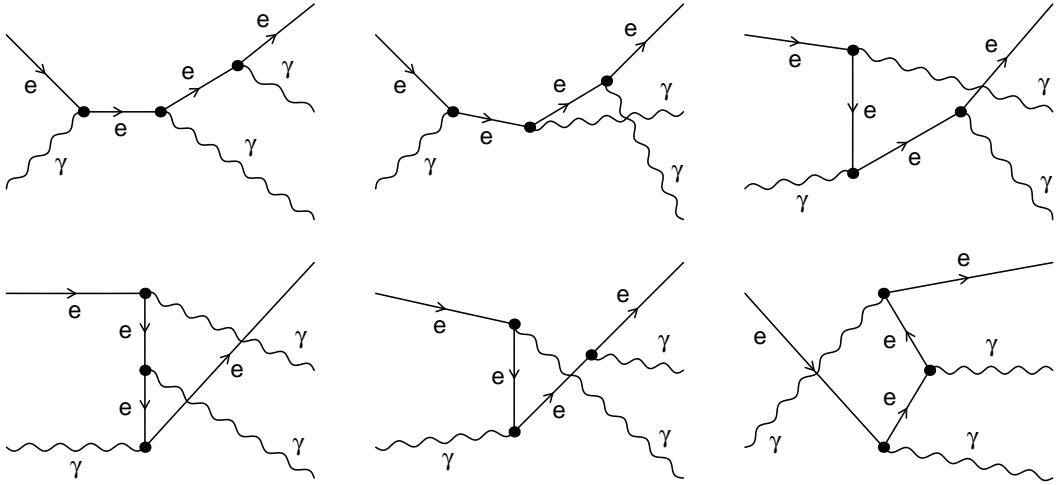


Figure 4: Tree diagrams for  $e^- \gamma \rightarrow e^- \gamma \gamma$ .

Figure 4 shows the tree diagrams describing double Compton scattering in lowest order. In terms of Weyl-van der Waerden spinor products the independent transition-matrix elements for  $\kappa = -1/2$  read

$$\begin{aligned} \mathcal{M}^-(+1, -1, -1) &= \mathcal{M}^-(+1, +1, +1) = 0, \\ \mathcal{M}^-(+1, +1, +1) &= 2\sqrt{2}ie^3 \frac{\langle p_e k_\gamma \rangle^* (\langle p'_e k_\gamma \rangle)^2 \langle p_e p'_e \rangle}{\langle p_e k_\gamma \rangle \langle p'_e k_1 \rangle^* \langle p_e k_1 \rangle \langle p'_e k_2 \rangle^* \langle p_e k_2 \rangle}, \\ \mathcal{M}^-(+1, +1, +1) &= 2\sqrt{2}ie^3 \frac{\langle p'_e k_\gamma \rangle (\langle p_e k_\gamma \rangle)^2 \langle p_e p'_e \rangle^*}{\langle p'_e k_\gamma \rangle^* \langle p'_e k_1 \rangle^* \langle p_e k_1 \rangle \langle p'_e k_2 \rangle^* \langle p_e k_2 \rangle}, \end{aligned} \quad (15)$$

where the spinorial products  $\langle \phi \psi \rangle$  are defined like in [12]. Moreover it is instructive to express the invariant spinor products of (15) in terms of particle energies ( $E, E'_e, E_1, E_2$ ) and scattering angles for the squared matrix elements:

$$\begin{aligned} |\mathcal{M}^-(+1, +1, +1)|^2 &= 2e^6 \frac{E E'_e \cos^4 \frac{\theta'_e}{2} \sin^2 \frac{\theta'_e}{2}}{E_1^2 E_2^2 \sin^2 \frac{\theta_1}{2} \sin^2 \frac{\theta_2}{2} \sin^2 \frac{\alpha_1}{2} \sin^2 \frac{\alpha_2}{2}}, \\ |\mathcal{M}^-(+1, +1, +1)|^2 &= 2e^6 \frac{E^3 \sin^2 \frac{\theta'_e}{2}}{E'_e E_1^2 E_2^2 \sin^2 \frac{\theta_1}{2} \sin^2 \frac{\theta_2}{2} \sin^2 \frac{\alpha_1}{2} \sin^2 \frac{\alpha_2}{2}}, \end{aligned} \quad (16)$$

with  $\theta'_e, \theta_i$  ( $i = 1, 2$ ) denoting the polar angles of the corresponding particles with respect to the direction of the incoming electron and  $\alpha_i = \angle(\mathbf{k}_i, \mathbf{p}'_e)$ . From (16) we can read for instance the structure of the IR and collinear poles in  $E_i, \theta_i$  and  $\alpha_i$ , respectively, which is different for the single polarization combinations. On the other hand all amplitudes contain the global factor  $\sin^2 \frac{\theta'_e}{2}$  so that non-collinear double Compton scattering is suppressed for forward scattering of the electron ( $\theta'_e \rightarrow 0$ ).

## 4.2 Collinear photon emission – finite-mass effects

One possible way to include the finite-mass effects of the electrons in the case of collinear photon emission has been proposed in [16]. This method is based on the introduction of *mass-effective factors*

$$\begin{aligned} f_+^{(\text{ini/fin})}(\xi, \varepsilon, \theta) &= \left( \frac{4\varepsilon^2 \sin^2 \frac{\theta}{2}}{4\varepsilon^2 \sin^2 \frac{\theta}{2} + m_e^2} \right)^2, \\ f_-^{(\text{ini/fin})}(\xi, \varepsilon, \theta) &= \frac{\xi^2}{\xi^2 \mp 2\xi + 2} \frac{4\varepsilon^2 m_e^2 \sin^2 \frac{\theta}{2}}{\left( 4\varepsilon^2 \sin^2 \frac{\theta}{2} + m_e^2 \right)^2}. \end{aligned} \quad (17)$$

for each initial/final-state electron of energy  $\varepsilon \gg m_e$  emitting a photon of energy  $\xi\varepsilon$ . Note that the functions  $f_+$  and  $f_-$  are different from 1 and 0, respectively, only for emission angles  $\theta \sim m_e/\varepsilon$ . In this collinear region the singular behaviour of  $|\mathcal{M}|^2$  for  $m_e = 0$  is replaced by the correct asymptotics via

$$\begin{aligned} \sum_{\lambda_1, \lambda_2 = \pm 1} |\mathcal{M}(\sigma_e, \sigma'_e, \lambda_\gamma, \lambda_1, \lambda_2)|^2 \Big|_{m_e \neq 0} &= \sum_{\substack{\kappa_1, \kappa'_1 = \pm 1 \\ \kappa_2, \kappa'_2 = \pm 1}} \left( \prod_{i=1,2} f_{\kappa_i}^{(\text{ini})}(x_i, E, \theta_i) f_{\kappa'_i}^{(\text{fin})}(x'_i, E'_e, \alpha_i) \right) \\ &\times \sum_{\lambda_1, \lambda_2 = \pm 1} |\mathcal{M}(\kappa_1 \kappa_2 \sigma_e, \kappa'_1 \kappa'_2 \sigma'_e, \lambda_\gamma, \lambda_1, \lambda_2)|^2 \Big|_{m_e=0} \\ \text{with: } x_i &= E_i/E, \quad x'_i = E_i/E'_e, \quad i = 1, 2. \end{aligned} \quad (18)$$

In this context we should mention that (18) is not valid for double collinear photon emission. However, this situation can not occur if we impose an angular cut  $\theta_e^{\text{for}} < \theta'_e < \theta_e^{\text{back}}$  on the electron scattering angle. Consequently in this angular region the spins of the electrons can not be flipped twice, in other words there will be no contributions to the sum in (18) if more than one of the  $\kappa_{1,2}^{(\prime)}$  are equal to  $-1$ .

Following this method of mass-effective factors collinearly emitted photons are included by suitable modifications of the squared amplitude so that the photon phase space is not restricted. In Sect. 4.4 we will describe an alternative method where the collinear regions of the phase space are treated separately.

## 4.3 Phase-space integration

In the CMS the total cross-section for double Compton scattering is given by

$$\sigma_{\text{tot}} = \frac{1}{8E^2} \sum_{\substack{\sigma_e, \lambda_\gamma \\ \sigma'_e, \lambda_1, \lambda_2}} \frac{1}{2} (1 + 2P_e \sigma_e) \frac{1}{2} (1 + P_\gamma \lambda_\gamma) \int_\Gamma d\Gamma |\mathcal{M}(\sigma_e, \sigma'_e, \lambda_\gamma, \lambda_1, \lambda_2)|^2. \quad (19)$$

Figure 5 illustrates the particle kinematics where  $\mathbf{k}_1$  is oriented into the  $x$ - $z$  plane making use of rotational invariance around the beam axis.  $\alpha_1$  and  $\beta$  denote the polar and azimuthal angle of  $\mathbf{p}'_e$  relative to  $\mathbf{k}_1$ , respectively.

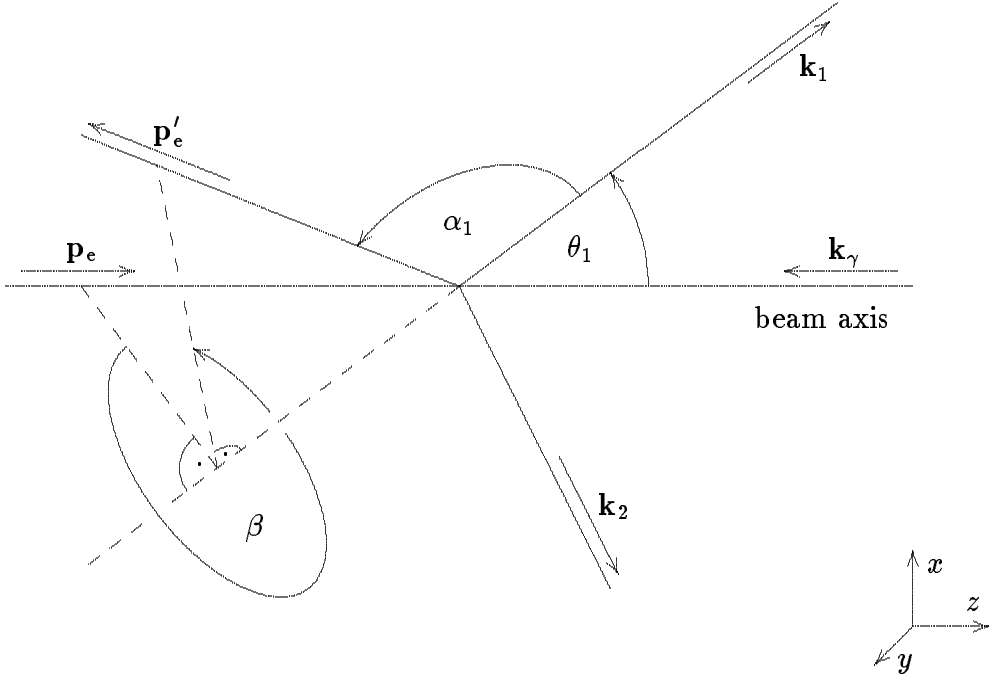


Figure 5: Particle kinematics for  $\phi_1 = 0$ .

$$\mathbf{p}'_e = E'_e \begin{pmatrix} \cos \theta_1 & 0 & \sin \theta_1 \\ 0 & 1 & 0 \\ -\sin \theta_1 & 0 & \cos \theta_1 \end{pmatrix} \begin{pmatrix} \cos \beta \sin \alpha_1 \\ \sin \beta \sin \alpha_1 \\ \cos \alpha_1 \end{pmatrix} \quad \text{for } \phi_1 = 0. \quad (20)$$

Owing to the fact that the two emitted photons are identical particles we have to symmetrize the polarized cross-sections and to apply a factor  $1/2$  when integrating over the photon phase space. Instead of this factor  $1/2$  we prefer to impose the constraint

$$E_1 \sin \frac{\theta_1}{2} \sin \frac{\alpha_1}{2} < E_2 \sin \frac{\theta_2}{2} \sin \frac{\alpha_2}{2} \quad (21)$$

which cuts the phase space in half in a symmetric way. Moreover (21) ensures that only photon ‘1’ may become an ‘IR’ or ‘collinear photon’. For this reason we choose the following parametrization for the phase space

$$\begin{aligned} \int_{\Gamma} d\Gamma &= \int \frac{d^3 \mathbf{p}'_e}{(2\pi)^3 2p'_e} \int \frac{d^3 \mathbf{k}_1}{(2\pi)^3 2k_1^0} \int \frac{d^3 \mathbf{k}_2}{(2\pi)^3 2k_2^0} (2\pi)^4 \delta^{(4)}(p_e + k_{\gamma} - p'_e - k_1 - k_2) \\ &= \frac{1}{8(2\pi)^5} \int dE_1 d\Omega_1 d\beta d\cos \alpha_1 \left| \frac{\partial E'_e}{\partial \cos \alpha_1} \right|, \end{aligned} \quad (22)$$

with

$$\frac{\partial E'_e}{\partial \cos \alpha_1} = -\frac{E_1 E (E - E_1)}{2 \left( E - E_1 \sin^2 \frac{\alpha_1}{2} \right)^2}, \quad (23)$$

which singles out both collinear singularities ( $\theta_1 \rightarrow 0, \alpha_1 \rightarrow 0$ ) as well as the IR pole ( $E_1 \rightarrow 0$ ). Furthermore these poles of the integrands have been transformed away by

appropriate transformations since numerical integration works best for flat functions. We have applied the well-known Monte Carlo routine *VEGAS* [17].

Apart from the different cuts the integration boundary is given by

$$0 \leq \theta_1 \leq \pi, \quad 0 \leq \beta \leq 2\pi, \quad 0 \leq \alpha_1 \leq \pi, \quad 0 \leq E_1 \leq E, \quad (24)$$

while the integration over  $\phi_1$  trivially yields a factor  $2\pi$ . In order to resolve the electron and at least one photon in the final state we restrict the phase space by

$$\begin{aligned} \theta_e^{\text{for}} &< \theta'_e < \theta_e^{\text{back}}, & E'_e &> \delta_e E, \\ \theta_\gamma^{\text{for}} &< \theta_i < \theta_\gamma^{\text{back}}, & E_i &> \delta_\gamma E \quad \text{for } i = 1 \text{ or } i = 2. \end{aligned} \quad (25)$$

## 4.4 Integration over the collinear regions

In [12] the integration over the collinear regions has been carried out analytically both for initial and final-state radiation. Here we can directly make use of the results given there and obtain for collinear initial-state radiation, i.e. for emission angles  $\theta_1 < \Delta\theta_1 \ll 1$ , the following integral representation:

$$\begin{aligned} \sigma_{\text{tot}}^{\text{coll,in}}(E) = \frac{\alpha}{2\pi} \left\{ (L_e - 1) \int_{x_{\text{min}}}^{x_{\text{max}}} dx \frac{x^2 - 2x + 2}{x} \hat{\sigma}_{\text{tot}}^{(x)}(\sqrt{1-x}E) \right. \\ \left. + \int_{x_{\text{min}}}^{x_{\text{max}}} dx x \hat{\sigma}_{\text{tot}}^{(x)}(\sqrt{1-x}E) \Big|_{P_e \rightarrow -P_e} \right\}, \end{aligned} \quad (26)$$

with

$$L_e = \log \left( \frac{\Delta\theta_1^2 E^2}{m_e^2} \right). \quad (27)$$

Of course the mass-singular logarithm  $\log m_e$  of (26) agrees with the one predicted in [15]. While the lower limit for  $x$  is simply set by the soft-photon cut  $\Delta E \ll E$  the determination of the maximal  $x$  is more complicated. The various energy and angular cuts (25) lead to

$$x_{\text{min}} = \frac{\Delta E}{E}, \quad x_{\text{max}} = \min \left\{ \frac{1 - \delta_e}{1 - \delta_e \sin^2 \frac{\theta_e^{\text{back}}}{2}}, \frac{1 - \delta_\gamma}{1 - \delta_\gamma \sin^2 \frac{\theta_\gamma^{\text{back}}}{2}} \right\}. \quad (28)$$

In (26)  $\hat{\sigma}_{\text{tot}}^{(x)}(\sqrt{1-x}E)$  represents the Born cross-section of the ‘hard process’  $e^- \gamma \rightarrow e^- \gamma$  which is transformed into the boosted CMS of  $(1-x)p_e$  and  $k_\gamma$  and calculated by integrating the differential cross-sections (2) with the beam energy  $E^{(x)} = \sqrt{1-x}E$  over the scattering angle  $\theta^{(x)}$  in the boosted system.  $\theta^{(x)}$  is related to  $\theta'_e$  and  $\theta_2$  by

$$\cos \theta^{(x)} = \frac{2 \cos \theta'_e + x(1 - \cos \theta'_e)}{2 - x(1 - \cos \theta'_e)} = -\frac{2 \cos \theta_2 + x(1 - \cos \theta_2)}{2 - x(1 - \cos \theta_2)}, \quad (29)$$

which transforms  $\theta_e^{\text{for/back}}$  and  $\theta_\gamma^{\text{for/back}}$  into the ( $x$ -dependent) angular cuts  $\theta_e^{(x),\text{for/back}}$  and  $\theta_\gamma^{(x),\text{for/back}}$  in the boosted system, respectively. However, the cut-offs  $\delta_e$  and  $\delta_\gamma$  for the particle energies influence the angular range  $I^{(x)}$  for  $\theta^{(x)}$ , too. Defining

$$\begin{aligned} \cos \hat{\theta}_e^{(x)} &= \frac{2}{x} \left( 1 - \frac{x}{2} - \delta_e \right) \quad \text{for } x > 1 - \delta_e, \\ \cos \hat{\theta}_\gamma^{(x)} &= -\frac{2}{x} \left( 1 - \frac{x}{2} - \delta_\gamma \right) \quad \text{for } x > 1 - \delta_\gamma, \end{aligned} \quad (30)$$

$I^{(x)}$  is given by

$$I^{(x)} = \left( \max \left\{ \theta_e^{(x),\text{for}}, \hat{\theta}_e^{(x)}, \theta_\gamma^{(x),\text{back}} \right\}, \min \left\{ \theta_e^{(x),\text{back}}, \theta_\gamma^{(x),\text{for}}, \hat{\theta}_\gamma^{(x)} \right\} \right). \quad (31)$$

The case of collinear final-state radiation, which corresponds to an integration over  $\alpha_1 < \Delta\alpha_1 \ll 1$ , is less involved yielding

$$\begin{aligned} \sigma_{\text{tot}}^{\text{coll,fin}}(\sigma'_e, E) = & \frac{\alpha}{2\pi} \left\{ \hat{\sigma}_{\text{tot}}(\sigma'_e, E) \left[ \frac{1}{2}(1 - \delta_e)(5 + \delta_e) + \delta_e(2 + \delta_e) \log \delta_e - 4 \text{Li}_2(1 - \delta_e) \right. \right. \\ & \left. \left. + (\hat{L}_e - 1) \left( -2 \log \left( \frac{\Delta E}{E} \right) - \frac{1}{2}(1 - \delta_e)(3 + \delta_e) + 2 \log(1 - \delta_e) \right) \right] \right. \\ & \left. + \hat{\sigma}_{\text{tot}}(-\sigma'_e, E) \frac{1}{2}(1 - \delta_e)^2 \right\}, \end{aligned} \quad (32)$$

with

$$\hat{L}_e = \log \left( \frac{\Delta\alpha_1^2 E^2}{m_e^2} \right). \quad (33)$$

Here  $\hat{\sigma}_{\text{tot}}(\sigma'_e, E)$  represents the Born cross-section for  $e^- \gamma \rightarrow e^- \gamma$  in the original CMS rendering the introduction of angular cuts trivial.

## 5 Results and discussion

### 5.1 Photonic corrections to $e^- \gamma \rightarrow e^- \gamma$

Since we adopt the input parameters from [5, 8, 12] for numerical evaluations all results fit properly to the ones given there. The investigation of hard-bremsstrahlung corrections to polarized Compton scattering is complicated by the fact that both emitted photons may become ‘IR’ or ‘collinear photons’. Although all given analytical results are sufficient for a discussion of completely polarized final states here we sum over both helicities  $\lambda_i = \pm 1$  ( $i = 1, 2$ ) and integrate over all singular regions of the phase space. In accordance with (25) the angular regions are restricted by  $\Delta\theta_e < \theta'_e < 180^\circ - \Delta\theta_e$  and  $\Delta\theta_\gamma < \theta_i < 180^\circ - \Delta\theta_\gamma$  for  $i = 1$  or  $i = 2$ . The energy cuts  $\Delta E_\gamma$  and  $\Delta E'_e$  are both adjusted to the beam energy  $E$  according to  $\Delta E_\gamma = \delta_\gamma E$  and  $\Delta E'_e = \delta_e E$  with the sample values  $\delta_\gamma = \delta_e = 0.2$ .

Figure 6 shows the total cross-sections for the helicity-changing channels ( $\kappa = \sigma_e = -\sigma'_e$ ) for the two different angular cuts  $\Delta\theta_\gamma = \Delta\theta_e = 20^\circ$  and  $\Delta\theta_\gamma = 0^\circ$ ,  $\Delta\theta_e = 1^\circ$ . As already observed for  $e^- \gamma \rightarrow W^- \nu_e \gamma$ ,  $e^- Z \gamma$  [12] these contributions are entirely due to collinear photon emission and can be calculated via (26) and (32). Inspecting these formulae we find that the considered cross-sections are independent of the electron mass. Consequently there is no intrinsic mass scale at all and  $\sigma_{\text{tot}}(\sigma_e = -\sigma'_e)$  is proportional to  $E^{-2}$  contributing several per mil to the unpolarized cross-section.

For the evaluation of the hard-photonic bremsstrahlung corrections to the helicity-conserving channels ( $\kappa = \sigma_e = \sigma'_e$ ) the full phase-space integration including also the non-collinear regions has to be performed. Instead of applying (18) we prefer to calculate the finite-mass effects using the results of Sect. 4.4. More precisely we exclude the collinear

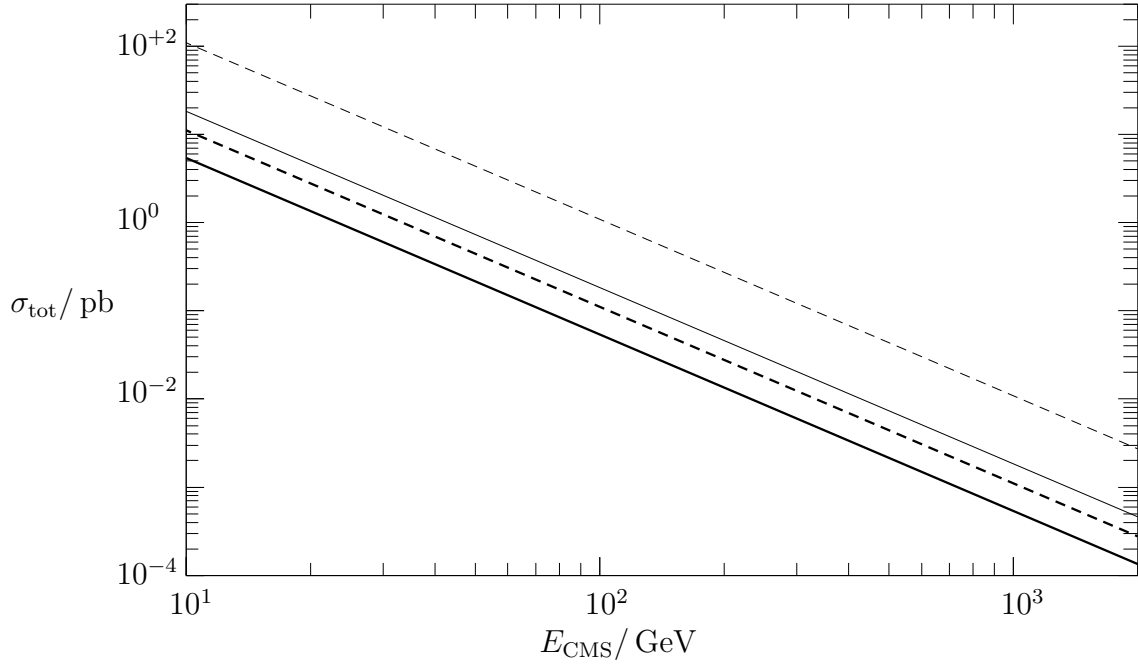


Figure 6: Cross-sections for helicity-changing channels ( $\kappa = \sigma_e = -\sigma'_e$ ) and polarizations ( $\kappa, \lambda_\gamma$ ) integrated with  $\Delta\theta_\gamma = \Delta\theta_e = 20^\circ$  (thick curves) and  $\Delta\theta_\gamma = 0^\circ, \Delta\theta_e = 1^\circ$ : — ( $\mp\frac{1}{2}, -1$ ), — — ( $\mp\frac{1}{2}, +1$ ).

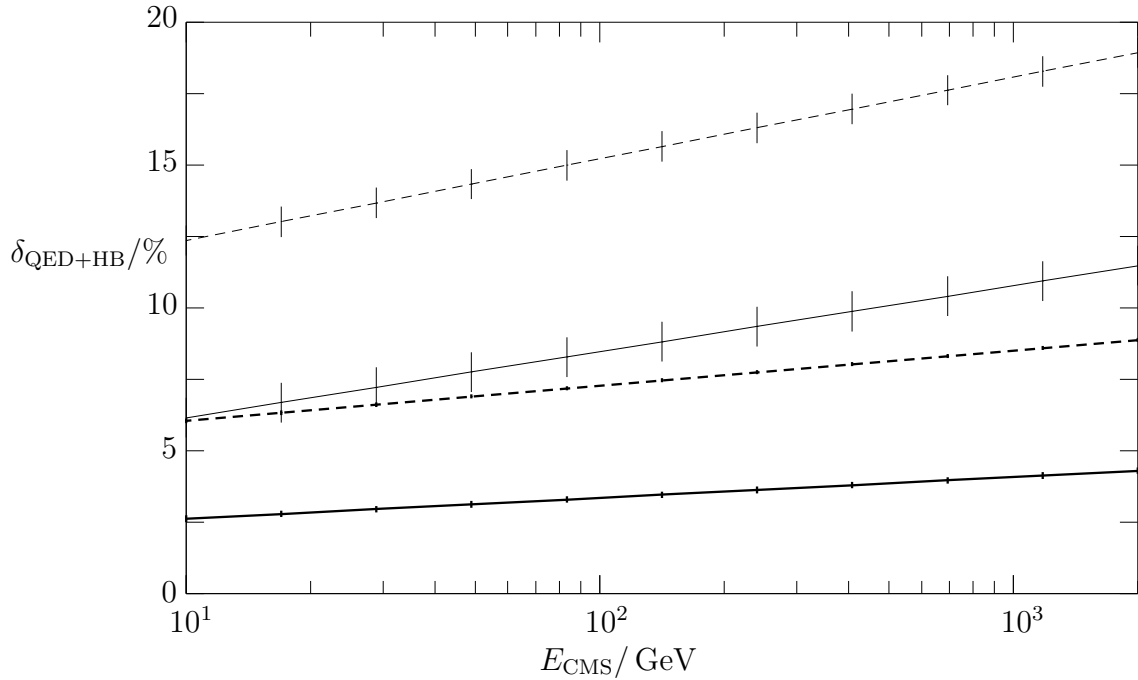


Figure 7: Photonic corrections to the integrated cross-section for different polarization combinations ( $\kappa, \lambda_\gamma$ ) with  $\kappa = \sigma_e = \sigma'_e$  (Same signature as Fig. 6).

regions  $\theta_i < \Delta\theta_i \ll 1$ ,  $\alpha_i < \Delta\alpha_i \ll 1$  ( $i = 1, 2$ ) from the phase-space integration and add the explicit results of (26) and (32) for the finite-mass effects. We define the hard-photonic corrections by

$$\delta_{\text{HB}} = \frac{\sigma_{\text{tot}}^{\text{e}^-\gamma \rightarrow \text{e}^-\gamma\gamma} \Big|_{E_{1,2} > \Delta E}}{\sigma_{\text{tot}}^{\text{e}^-\gamma \rightarrow \text{e}^-\gamma}} \quad (34)$$

and combine them with the virtual and real soft-photonic QED corrections  $\delta_{\text{QED}}$  of Sect. 3

$$\delta_{\text{QED+HB}} = \delta_{\text{HB}} + \delta_{\text{QED}} = \delta_{\text{HB}} + \delta_{\text{QED}}^{\text{virt}} + \delta_{\text{SB}}. \quad (35)$$

Hence the gauge-invariant, IR-finite, and  $\Delta E$ -independent factor  $\delta_{\text{QED+HB}}$  consists of all photonic corrections to  $\text{e}^-\gamma \rightarrow \text{e}^-\gamma$ .

$\delta_{\text{QED+HB}}$ , which is illustrated in Fig. 7 for the single polarization combinations  $(\kappa, \lambda_\gamma)$ , turns out to be at the (positive) per-cent level and increases with decreasing cuts for  $\theta_i$  and  $\theta'_e$ . Here and in the following figures the error bars of the Monte Carlo statistics are indicated by vertical lines on the corresponding curves. As already observed for  $\text{e}^-\gamma \rightarrow \text{e}^-Z\gamma$  [12] the u-channel pole of the cross-sections causes a reduction of the numerical accuracy for very small cuts  $\Delta\theta_e$ . However, the case  $\Delta\theta_e = 1^\circ$  is not of physical relevance, but it is considered just for illustrating the influence of this cut-off. Since the only dependence on the electron mass  $m_e$  is logarithmic the photonic corrections are of the form

$$\delta_{\text{QED+HB}} = C_1 + C_2 \log\left(\frac{m_e}{E}\right), \quad C_i = \text{const.}, \quad i = 1, 2, \quad (36)$$

for fixed cut-off parameters  $\Delta\theta_\gamma$ ,  $\Delta\theta_e$ ,  $\delta_\gamma$ ,  $\delta_e$ . Consequently the numerical integration over the three-particle phase space for non-collinear photon emission yields a constant contribution to  $\delta_{\text{HB}}$  and has to be performed only once for each curve of Fig. 7 as the energy-dependent term of  $\delta_{\text{HB}}$  is contained in the collinearity parts.

As we have checked analytically as well as numerically all results for  $\text{e}^-\gamma \rightarrow \text{e}^-Z\gamma$  [12] hold for  $\text{e}^-\gamma \rightarrow \text{e}^-\gamma\gamma$  after substituting  $M_Z \rightarrow 0$ ,  $g_{\text{ee}Z}^\kappa \rightarrow g_{\text{ee}\gamma}^\kappa = 1$ . Moreover we have verified that the results for  $\delta_{\text{QED+HB}}$  do not depend on the auxiliary IR ( $\Delta E$ ) and angular cuts ( $\Delta\theta_i$ ,  $\Delta\alpha_i$ ). This fact is demonstrated in Table 1, where the photonic corrections are listed for various cut-offs together with the corresponding statistical errors and the  $\chi^2$  per degrees of freedom given by *VEGAS*. In particular a second version for the calculation of these corrections ( $\delta'_{\text{QED+HB}}$ ) is also included there which follows the method of mass-effective factors outlined in Sect. 4.2.

## 5.2 Full $\mathcal{O}(\alpha)$ electroweak corrections to $\text{e}^-\gamma \rightarrow \text{e}^-\gamma$

The full  $\mathcal{O}(\alpha)$  corrections to Compton scattering are furnished by the photonic contributions of the previous section together with the virtual electroweak RCs given in Sect. 3

$$\delta_{\text{full}} = \delta_{\text{QED+HB}} + \delta_{\text{weak}} = \delta_{\text{QED+HB}} + \delta_{\text{NC}} + \delta_{\text{W}}. \quad (37)$$

Since the results for  $\delta_{\text{weak}}$  have already been discussed in detail in [5] we immediately turn to  $\delta_{\text{full}}$ , which is illustrated in Fig. 8 for the electron-helicity-conserving channels ( $\kappa = \sigma_e = \sigma'_e$ ). For energies below the scale of the weak gauge bosons  $\delta_{\text{full}}^{+\kappa} (+\lambda_\gamma)$  and

$\Delta E/E$	$\Delta\theta_{1,2}, \Delta\alpha_{1,2}$	$\delta_{\text{QED+HB}}/\%$	$\sigma_{\text{st.dev.}}/\%$	$\chi^2$	$\delta'_{\text{QED+HB}}/\%$	$\sigma'_{\text{st.dev.}}/\%$	$\chi'^2$
$10^{-3}$	$10^{-3}$	4.05	0.11	0.23	4.09	0.17	0.88
	$10^{-5}$	4.09	0.17	0.27			
	$10^{-7}$	4.12	0.24	0.79			
$10^{-5}$	$10^{-3}$	4.01	0.17	0.37	4.17	0.27	0.56
	$10^{-5}$	4.00	0.27	0.31			
	$10^{-7}$	4.17	0.40	0.43			
$10^{-7}$	$10^{-3}$	3.94	0.24	0.58	4.27	0.38	0.59
	$10^{-5}$	4.34	0.39	0.42			
	$10^{-7}$	4.32	0.55	0.37			

Table 1: Cutoff (in-)dependence of the photonic corrections to the unpolarized cross-section of  $e^- \gamma \rightarrow e^- \gamma$  for  $E_{\text{CMS}} = 100 \text{ GeV}$  and  $\Delta\theta_e, \Delta\theta_\gamma = 20^\circ$ .

$\delta_{\text{full}}^{-\kappa}(-\lambda_\gamma)$  coincide as the (parity-non-conserving) weak corrections  $\delta_{\text{weak}}$  do not yield sizeable contributions there and we are left with the pure (parity-conserving) photonic corrections  $\delta_{\text{QED+HB}}$ . For energies above the threshold singularity at  $E_{\text{CMS}} = M_Z$ , which shows up as a tiny (logarithmic) peak, considerable (negative) weak corrections arise for left-handed electrons which even exceed the (positive) photonic corrections of pure QED for several hundred GeV. On the other hand  $\delta_{\text{weak}}^+$  hardly contributes to  $\delta_{\text{full}}^+$  for right-handed electrons. Altogether the RCs in  $\mathcal{O}(\alpha)$  to the polarized Compton cross-sections are of the order  $\lesssim 10\%$  for energies between 10 GeV and 2 TeV.

The full  $\mathcal{O}(\alpha)$  RCs to the unpolarized cross-section are compared to the photonic corrections in Fig. 9. While Compton scattering represents practically a pure electromagnetic process for energies below  $M_Z$  the (negative) weak corrections exceed the (positive) photonic corrections in the TeV range. From Fig. 9 we can also deduce that the  $\mathcal{O}(\alpha)$  RCs are the more enhanced the more tiny we choose the angular cuts  $\Delta\theta_\gamma$  and  $\Delta\theta_e$ . Finally the single contributions of the weak and photonic RCs to  $\delta_{\text{full}}$  are summarized in Table 2 where we have again compared the two versions  $\delta_{\text{QED+HB}}^{(i)}$  for the photonic corrections.

Note that apart from a trivial normalization effect the polarization asymmetry of the incoming photon is not influenced by the photonic corrections  $\delta_{\text{QED+HB}}$  at all. Thus the weakly corrected polarization asymmetry, which is discussed in [5], is practically identical with the full  $\mathcal{O}(\alpha)$  corrected one.

## 6 Summary

Applying the computer-algebra packages *FeynArts* [9] and *FeynCalc* [10] we have calculated the virtual electroweak radiative corrections to high-energy Compton scattering. In

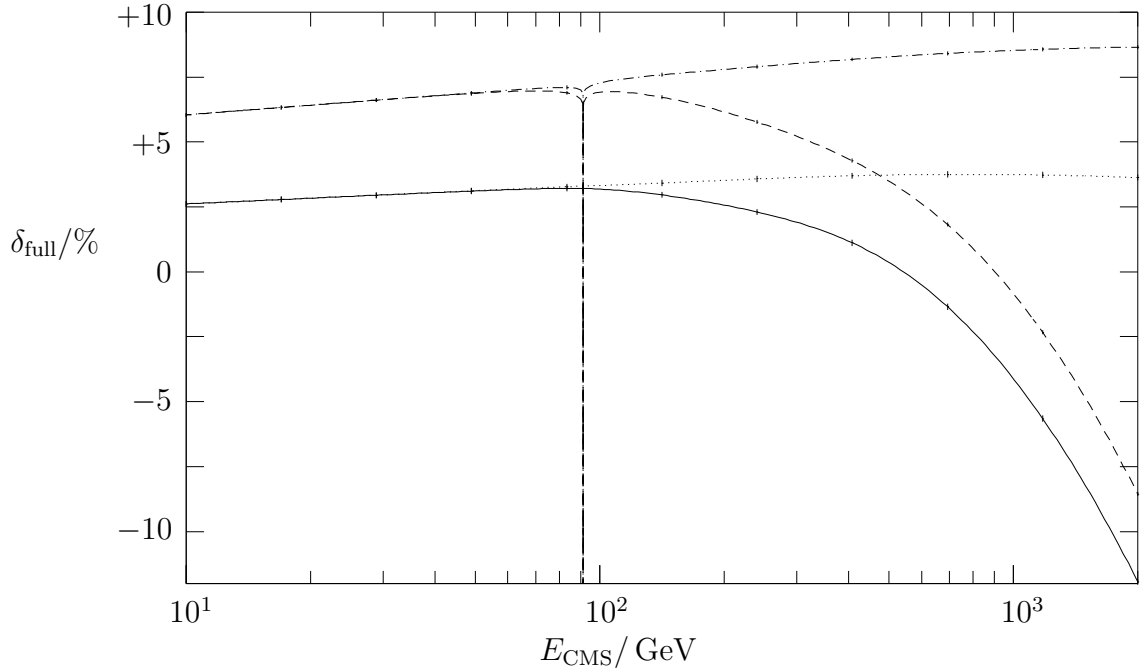


Figure 8: Full  $\mathcal{O}(\alpha)$  corrections to the integrated cross-section ( $\Delta\theta_e = \Delta\theta_\gamma = 20^\circ$ ) for different polarization combinations  $(\kappa, \lambda_\gamma)$  with  $\kappa = \sigma_e = \sigma'_e$ : —  $(-\frac{1}{2}, -1)$ , — — —  $(-\frac{1}{2}, +1)$ , ·····  $(+\frac{1}{2}, +1)$ , - · - -  $(+\frac{1}{2}, -1)$ .

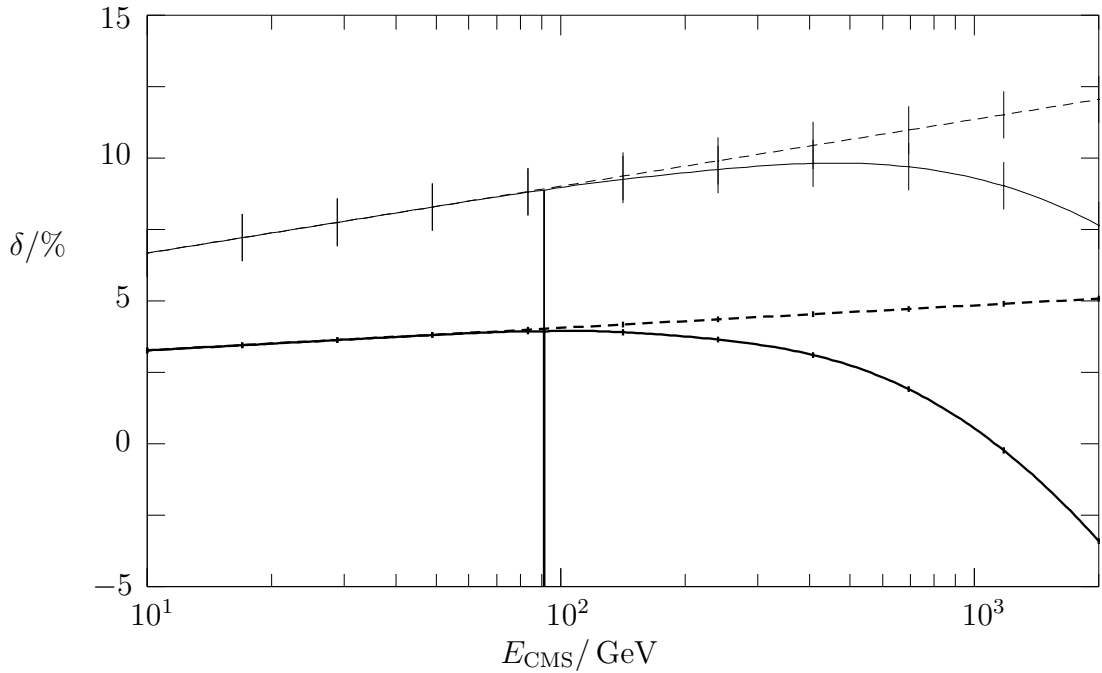


Figure 9: Full  $\mathcal{O}(\alpha)$  and photonic corrections to the unpolarized cross-section integrated with  $\Delta\theta_\gamma = \Delta\theta_e = 20^\circ$  (thick curves) and  $\Delta\theta_\gamma = 0^\circ$ ,  $\Delta\theta_e = 1^\circ$ : —  $\delta_{\text{full}}$ , — —  $\delta_{\text{QED+HB}}$ .

$E_{\text{CMS}}$	50 GeV		100 GeV		500 GeV		2 TeV	
$\Delta\theta_e/\Delta\theta_\gamma$	1°/0°	20°/20°	1°/0°	20°/20°	1°/0°	20°/20°	1°/0°	20°/20°
$\sigma_{\text{Born}}/\text{pb}$	520.226	205.363	130.057	51.341	5.202	2.054	0.3251	0.1284
$\delta_{\text{full}}/\%$	8.74 ±0.83	3.80 ±0.11	9.48 ±0.83	3.95 ±0.11	10.51 ±0.83	2.74 ±0.11	8.49 ±0.83	-3.42 ±0.11
$\delta_{\text{weak}}/\%$	-0.00	-0.01	-0.04	-0.10	-0.83	-1.86	-4.41	-8.49
$\delta_{\text{QED+HB}}/\%$	8.74 ±0.83	3.81 ±0.11	9.52 ±0.83	4.05 ±0.11	11.34 ±0.83	4.60 ±0.11	12.90 ±0.83	5.07 ±0.11
$\delta'_{\text{QED+HB}}/\%$	8.42 ±0.81	3.80 ±0.16	9.6 ±1.1	4.09 ±0.17	9.8 ±1.9	4.62 ±0.18	11.2 ±1.8	5.14 ±0.21

Table 2: Full, weak and photonic corrections to  $e^-\gamma \rightarrow e^-\gamma$  for the unpolarized cross-section.

comparison with the existing results of [5] the obtained analytical expressions turn out to be very simple and well-suited for numerical evaluations or further theoretical investigations. Moreover we have given compact results for the helicity amplitudes of double Compton scattering in terms of Weyl-van der Waerden spinor products valid for non-collinear photon emission. The inclusion of the corresponding finite-mass effects of the electron has been described in detail. Finally we have presented numerical results both for the purely photonic as well as for the full  $\mathcal{O}(\alpha)$  corrections to the integrated cross-section of  $e^-\gamma \rightarrow e^-\gamma$  for polarized and unpolarized particles. For energies ranging from 10 GeV to 2 TeV the corrections modify the lowest-order cross-sections roughly by 5 – 10%.

Together with the investigation of the virtual electroweak radiative corrections to  $e^-\gamma \rightarrow W^-\nu_e$ ,  $e^-\gamma \rightarrow e^-Z$ ,  $e^-\gamma \rightarrow e^-\gamma$  in [5, 8] and the radiative processes  $e^-\gamma \rightarrow W^-\nu_e\gamma$ ,  $e^-\gamma \rightarrow Z\gamma$  in [12] this work completes the discussion of gauge-boson production in electron-photon collisions up to the first order in  $\alpha$ . In view of experimental requirements further studies on this subject are desirable. In particular the angular distributions of the hard-photonic corrected cross-sections as well as the energy spectra of the hard photons should also be investigated.

## Acknowledgement

The author would like to thank A. Denner and H. Spiesberger for helpful discussions and advice.

# Appendix

## A List of scalar integrals

For completeness here we list all scalar one-loop integrals which have been used for the calculation of the virtual RCs given in Sect. 3. Following the conventions of [11] the scalar integrals are defined by:

$$\begin{aligned}
B_0(p_1^2, m_0, m_1) &= \frac{(2\pi\mu)^{4-D}}{i\pi^2} \int d^D q \frac{1}{[q^2 - m_0^2 + i\varepsilon][(q + p_1)^2 - m_1^2 + i\varepsilon]}, \\
C_0(p_1^2, (p_2 - p_1)^2, p_2^2, m_0, m_1, m_2) &= \frac{1}{i\pi^2} \int d^4 q \\
&\times \frac{1}{[q^2 - m_0^2 + i\varepsilon][(q + p_1)^2 - m_1^2 + i\varepsilon][(q + p_2)^2 - m_2^2 + i\varepsilon]}, \\
D_0(p_1^2, (p_2 - p_1)^2, (p_3 - p_2)^2, p_3^2, p_2^2, (p_3 - p_1)^2, m_0, m_1, m_2, m_3) &= \frac{1}{i\pi^2} \int d^4 q \\
&\times \frac{1}{[q^2 - m_0^2 + i\varepsilon][(q + p_1)^2 - m_1^2 + i\varepsilon][(q + p_2)^2 - m_2^2 + i\varepsilon][(q + p_3)^2 - m_3^2 + i\varepsilon]}. \quad (\text{A.1})
\end{aligned}$$

All needed 2-point functions  $B_0$ , which are calculated in  $D$  space-time dimensions with  $D \rightarrow 4$ , can be easily derived from the special cases:

$$\begin{aligned}
B_0(x, m, m) &= \Delta + 2 - \log\left(\frac{m^2}{\mu^2}\right) + \beta_{xm} \log\left(\frac{\beta_{xm} - 1}{\beta_{xm} + 1}\right), \quad \beta_{xm} = \sqrt{1 - \frac{4m^2}{x + i\varepsilon}}, \\
B_0(x, 0, m) &= \Delta + 2 - \log\left(\frac{m^2}{\mu^2}\right) + \left(\frac{m^2}{x} - 1\right) \log\left(1 - \frac{x + i\varepsilon}{m^2}\right). \quad (\text{A.2})
\end{aligned}$$

Of course all renormalized quantities do not depend on the arbitrary reference mass  $\mu$  and the constant

$$\Delta = \frac{2}{4 - D} - \gamma_E + \log 4\pi \quad (\text{A.3})$$

which contains the UV divergences. Except for the photonic contribution to the field-renormalization constant  $\delta Z^{e,\kappa}$  of the electron, which we have taken from [14], the  $B_0$  functions of (A.2) are also sufficient for the determination of the field-renormalization constants which contain  $\partial B_0 / \partial p^2$ . In particular the abbreviations  $B_{t\text{WW}}$ ,  $B_{s\text{0W}}$ , and  $B_{u\text{0W}}$  used in (3.3) are given by:

$$\begin{aligned}
B_{t\text{WW}} &= B_0(t, M_W, M_W) - B_0(0, M_W, M_W), \\
B_{v\text{0W}} &= B_0(v, 0, M_W) - B_0(0, 0, M_W), \quad v = s, u. \quad (\text{A.4})
\end{aligned}$$

The following 3- and 4-point functions are calculated for the limit  $s, -t, -u, M_W^2 \gg m_e^2$  where the infinitesimal photon mass  $\lambda$  regularizes possible IR divergences. Scalar functions

which are related by crossing symmetry ( $s \leftrightarrow u$ ) are given generically with the abbreviation  $r = s + i\varepsilon, u + i\varepsilon$ .

$$\begin{aligned}
C_0(m_e^2, 0, r, 0, m_e, m_e) &= \frac{1}{r} \left[ 2\zeta(2) + \frac{1}{2} \log^2 \left( \frac{m_e^2}{-r} \right) \right], \quad \zeta(2) = \frac{\pi^2}{6}, \\
C_0(m_e^2, m_e^2, t, m_e, \lambda, m_e) &= \frac{1}{t} \left[ \frac{1}{2} \log^2 \left( \frac{m_e^2}{-t} \right) + \log \left( \frac{m_e^2}{-t} \right) \log \left( \frac{\lambda^2}{m_e^2} \right) - \zeta(2) \right], \\
C_0(0, 0, t, m_e, m_e, m_e) &= \frac{1}{2t} \log^2 \left( \frac{m_e^2}{-t} \right), \\
C_0(m_e^2, 0, r, M_Z, m_e, m_e) &= \frac{1}{r} \left[ \text{Li}_2 \left( \frac{r}{M_Z^2} \right) - \log \left( \frac{m_e^2}{M_Z^2 - r} \right) \log \left( 1 - \frac{r}{M_Z^2} \right) \right], \\
C_0(0, 0, t, 0, M_Z, 0) &= \frac{1}{t} \left[ \zeta(2) - \text{Li}_2 \left( 1 + \frac{t}{M_Z^2} \right) \right], \\
C_0(0, 0, r, 0, M_W, M_W) &= C_{rWW} = -\frac{1}{r} \text{Li}_2 \left( \frac{r}{M_W^2} \right), \\
C_0(0, 0, t, M_W, 0, M_W) &= C_{tWW} = \frac{1}{t} \log^2 \left( \frac{\beta_{tW} + 1}{\beta_{tW} - 1} \right), \quad \beta_{tW} = \sqrt{1 - \frac{4M_W^2}{t}}, \\
C_0(0, 0, t, M_W, M_W, M_W) &= C_{tWWW} = \frac{1}{2t} \log^2 \left( \frac{\beta_{tW} + 1}{\beta_{tW} - 1} \right), \tag{A.5}
\end{aligned}$$

$$\begin{aligned}
D_0(0, m_e^2, 0, m_e^2, r, t, m_e, m_e, \lambda, m_e) &= \frac{1}{rt} \left[ 2 \log \left( \frac{m_e^2}{-t} \right) \log \left( \frac{\lambda m_e}{-r} \right) - 3\zeta(2) \right], \\
D_0(0, m_e^2, 0, m_e^2, r, t, m_e, m_e, M_Z, m_e) &= \frac{1}{t(r - M_Z^2)} \left[ -2 \log \left( \frac{m_e^2}{-t} \right) \log \left( 1 - \frac{r}{M_Z^2} \right) \right. \\
&\quad \left. + \frac{1}{2} \log^2 \left( \frac{-t}{m_e^2} \right) + \text{Li}_2 \left( 1 + \frac{t}{M_Z^2} \right) - 4 \text{Li}_2 \left( \frac{r}{r - M_Z^2} \right) - \zeta(2) \right], \\
D_0(0, 0, 0, 0, r, t, M_W, M_W, 0, M_W) &= D_{rt} = \frac{1}{\sqrt{t^2(r - M_W^2)^2 - 4r^2tM_W^2}} \sum_{n=1}^2 (-1)^{n+1} \\
&\quad \times \left[ \log \left( 1 - \frac{r}{M_W^2} \right) \log(-x_n) - \text{Li}_2 \left( 1 + \frac{\beta_{tW} + 1}{\beta_{tW} - 1} x_n \right) - \text{Li}_2 \left( 1 + \frac{\beta_{tW} - 1}{\beta_{tW} + 1} x_n \right) \right. \\
&\quad \left. + 3 \text{Li}_2(1 + x_n) - \text{Li}_2 \left( 1 + \frac{x_n M_W^2}{M_W^2 - r} \right) - \eta \left( -x_n, \frac{M_W^2}{M_W^2 - r} \right) \log \left( 1 + \frac{x_n M_W^2}{M_W^2 - r} \right) \right], \\
\text{with: } x_{1,2} &= \left[ t(r - M_W^2) - 2r \pm \sqrt{t^2(r - M_W^2)^2 - 4r^2tM_W^2} \right] / 2(r + t), \tag{A.6}
\end{aligned}$$

The dilogarithm  $\text{Li}_2(x)$  and the  $\eta$ -function  $\eta(x, y)$  are defined as usual

$$\text{Li}_2(x) = - \int_0^x \frac{dt}{t} \log(1 - t), \quad -\pi < \text{arc}(1 - x) < \pi, \tag{A.7}$$

$$\eta(x, y) = \log(xy) - \log(x) - \log(y), \quad -\pi < \text{arc}(x), \text{arc}(y) < \pi. \tag{A.8}$$

## References

- [1] A.H. Compton, *Phys. Rev.* **21** (1923) 715.
- [2] O. Klein and Y. Nishina, *Z. Phys.* **52** (1929) 853.
- [3] L.M. Brown and R.P. Feynman, *Phys. Rev.* **85** (1952) 231.
- [4] F. Mandl and T.H.R. Skyrme, *Proc. Roy. Soc. A* **215** (1952) 497.
- [5] A. Denner and S. Dittmaier, *Nucl. Phys.* **B407** (1993) 43.
- [6] S. Dittmaier, dissertation, University of Würzburg, 1993.
- [7] I.F. Ginzburg, G.L. Kotkin, V.G. Serbo and V.I. Telnov, *Nucl. Instr. Meth.* **205** (1983) 47;  
I.F. Ginzburg, G.L. Kotkin, S.L. Panfil, V.G. Serbo and V.I. Telnov, *Nucl. Instr. Meth.* **219** (1984) 5;  
D.L. Borden, D.A. Bauer and D.O. Caldwell, SLAC-PUB-5715, UCSB-HEP-92-01, submitted to *Phys. Rev. D*.
- [8] A. Denner and S. Dittmaier, *Nucl. Phys.* **B398** (1993) 239; **B398** (1993) 265.
- [9] J. Küblbeck, M. Böhm and A. Denner, *Comp. Phys. Comm.* **60** (1990) 165;  
H. Eck and J. Küblbeck, *Guide to FeynArts 1.0*, University of Würzburg, 1992.
- [10] R. Mertig, M. Böhm and A. Denner, *Comp. Phys. Comm.* **64** (1991) 345;  
R. Mertig, *Guide to FeynCalc 1.0*, University of Würzburg, 1992.
- [11] G. 't Hooft and M. Veltman, *Nucl. Phys.* **B153** (1979) 365;  
W. Beenakker and A. Denner, *Nucl. Phys.* **B338** (1990) 349;  
A. Denner, U. Nierste and R. Scharf, *Nucl. Phys.* **B376** (1991) 637.
- [12] M. Böhm and S. Dittmaier, *Nucl. Phys.* **B409** (1993) 3; *The hard-bremsstrahlung process  $e^- \gamma \rightarrow e^- Z \gamma$* , Würzburg preprint 1993; to appear in *Nucl. Phys. B*.
- [13] K.I. Aoki, Z. Hioki, R. Kawabe, M. Konuma and T. Muta, *Prog. Theo. Phys.* **64** (1980) 707; **65** (1981) 1001; *Suppl. Prog. Theo. Phys.* **73** (1982) 1.
- [14] A. Denner, Habilitation thesis, Würzburg (1991), *Fortschr. Phys.* **41** (1993) 307;  
M. Böhm and A. Denner, *Radiative Corrections in the Electroweak Standard Model*, in *Proceedings of the Workshop on High Energy Phenomenology*, Mexico City, 1991, eds. R. Huerta and M.A. Perez (World Scientific, Singapore, 1992), p. 1.
- [15] W. Beenakker, F.A. Berends and W.L. van Neerven, in *Radiative Corrections for  $e^+ e^-$  Collisions*, ed. J.H. Kühn (Springer, Berlin, 1989), p. 3.
- [16] F.A. Berends et al., *Nucl. Phys.* **B206** (1982) 53;  
R. Kleiss, *Z. Phys.* **33** (1987) 433.
- [17] G.P. Lepage, *J. Comp. Phys.* **27** (1978) 192; Cornell University preprint, CLNS-80/447 (1980).